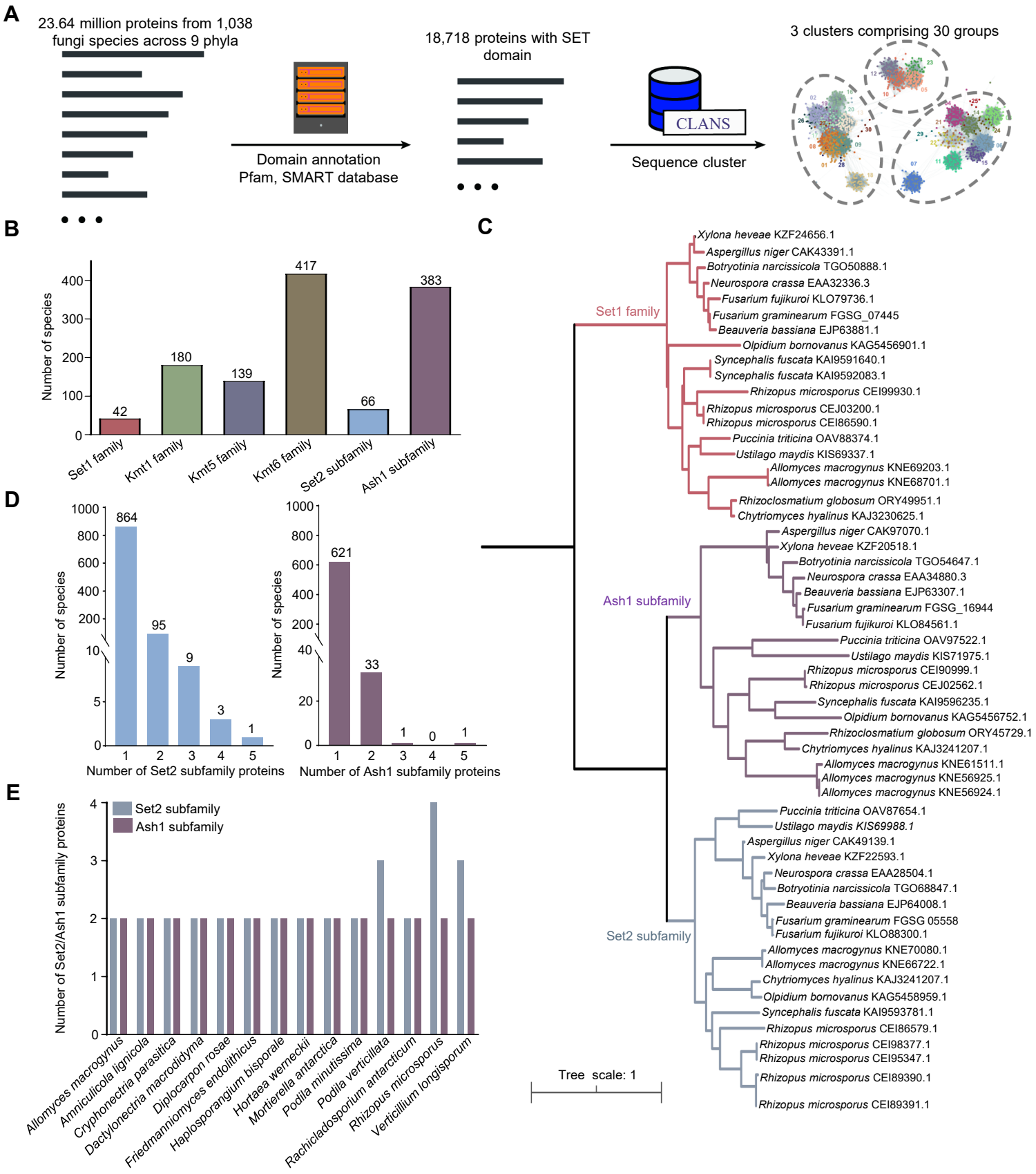

Supplemental Figure S1. Workflow for identifying SET domain proteins across the fungal kingdom and phylogeny of the Set2/Ash1 superfamily. (A) Workflow for identifying SET domain proteins in 1,038 fungal genomes and clustering by CLANS. (B) Counts of fungal species lacking specific histone methyltransferases (HMTs). (C) Maximum-likelihood phylogeny of Set2 and Ash1 subfamilies across representative fungal species; Set1 used as outgroup, Scale bar = 1. (D) Species counts by Set2/Ash1 copy number. (E) Fourteen species harboring ≥ 2 Set2 and ≥ 2 Ash1 copies.

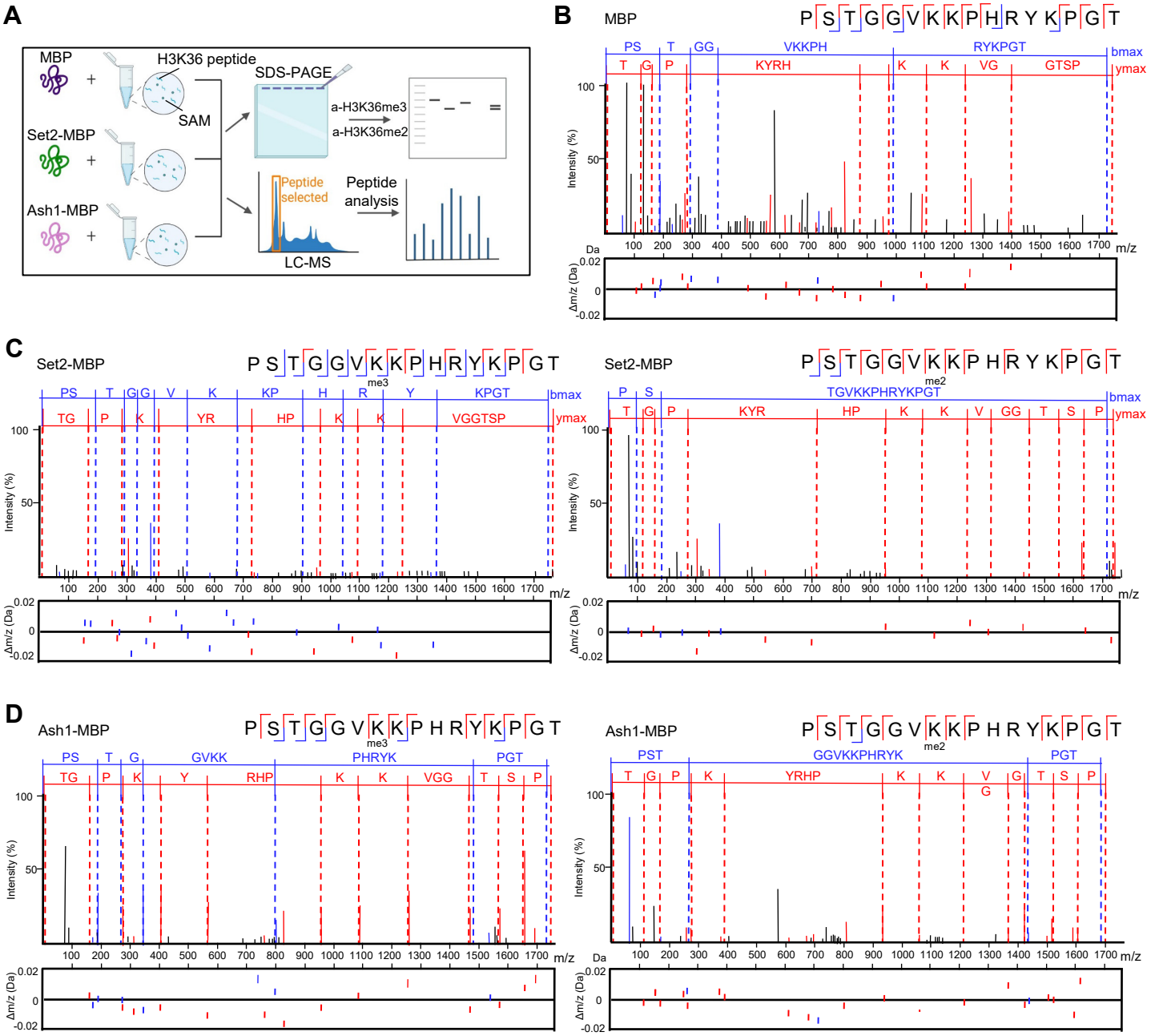

Supplemental Figure S2. Set2 and Ash1 catalyze *in vitro* methylation of an H3K36 peptide. (A) Assay schematic: purified Set2 (green trace), Ash1 (pink trace), or MBP control (purple trace) incubated with unmethylated H3K36 peptides (blue rectangles) and S-adenosyl-L-methionine (SAM, green circles) at 30 °C; reactions analyzed by SDS-PAGE or LC-MS. (B–D) CID/HCD MS/MS spectra and mass error (Δm/z) distributions for the peptide PSTGGVKKPHRYKPGT: (B) MBP, (C) Set2, (D) Ash1. b-/y-ions shown (top); errors -0.02 to +0.02 Da (bottom). Mass shifts of + 28.03 and + 42.05 Da at K7 indicate di- and trimethylation.

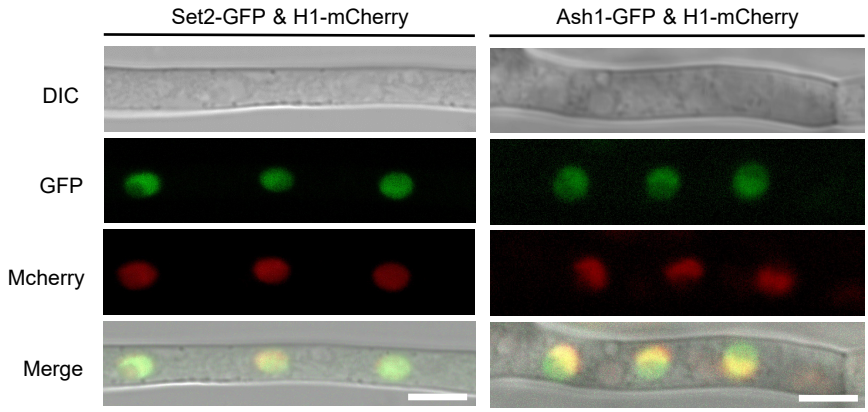

Supplemental Figure S3. Subcellular localization of Ash1-GFP and Set2-GFP in mycelia. Ash1-GFP and Set2-GFP were co-expressed with nuclear marker H1-mCherry in respective strains. Differential interference contrast (DIC), GFP, and mCherry fluorescence images are shown. Scale bars, 5 μm.

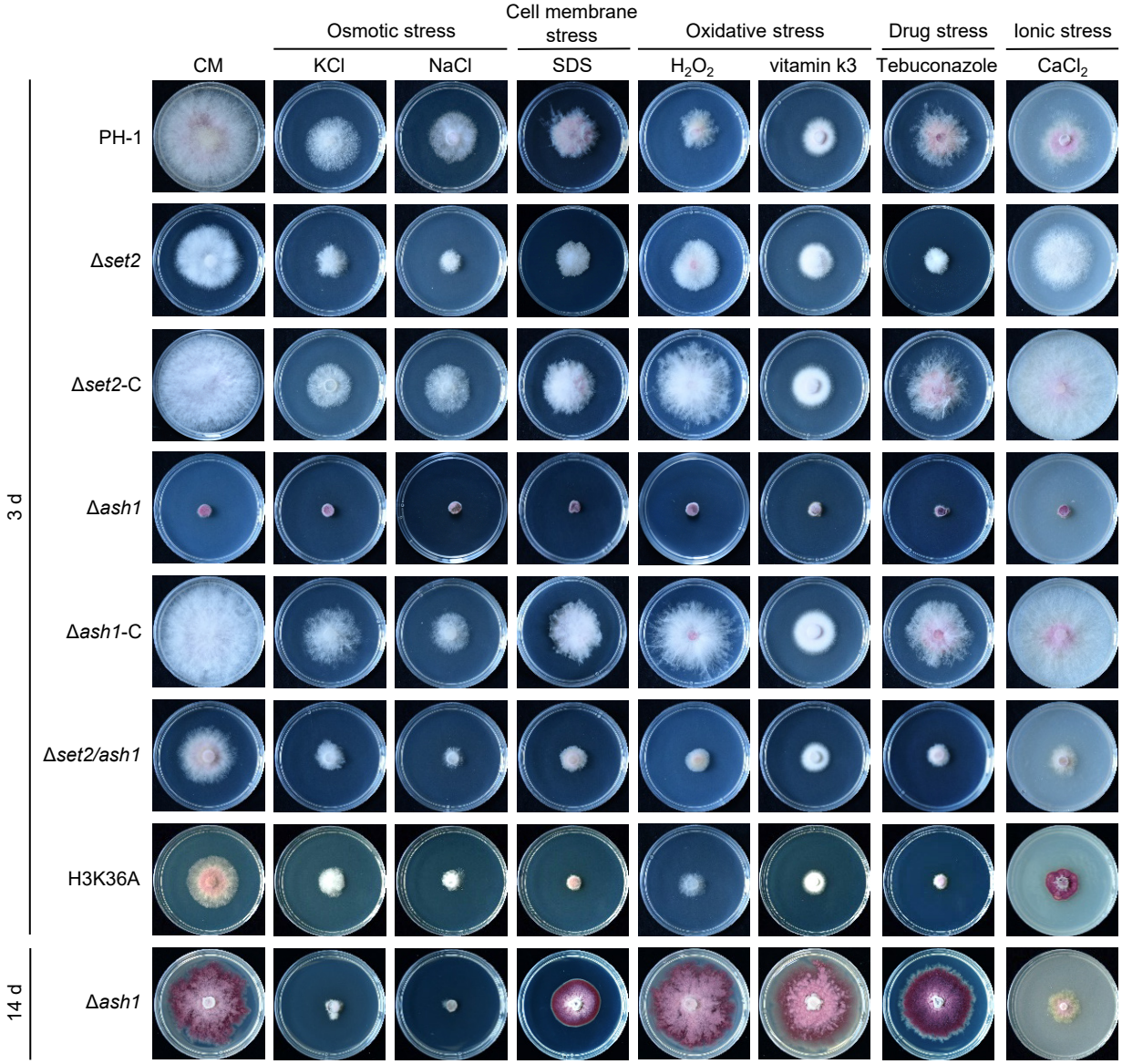

Supplemental Figure S4. Set2 and Ash1 contribute to stress responses in *F. graminearum*. Colony morphologies of PH-1, Δ*set2*, Δ*ash1*, Δ*set2*/*ash1*, and H3K36A on CM supplemented with stress agents: 0.25 ppm tebuconazole, 0.01% SDS, 1.2 M KCl, 1.2 M NaCl, 0.2 M $CaCl_2$, 0.05% H_2O_2 and 10 mM vitamin k3. PH-1, Δ*set2*, Δ*set2*/*ash1*, and H3K36A were photographed at 3 days; Δ*ash1* at days 3 and 14 due to slower growth.

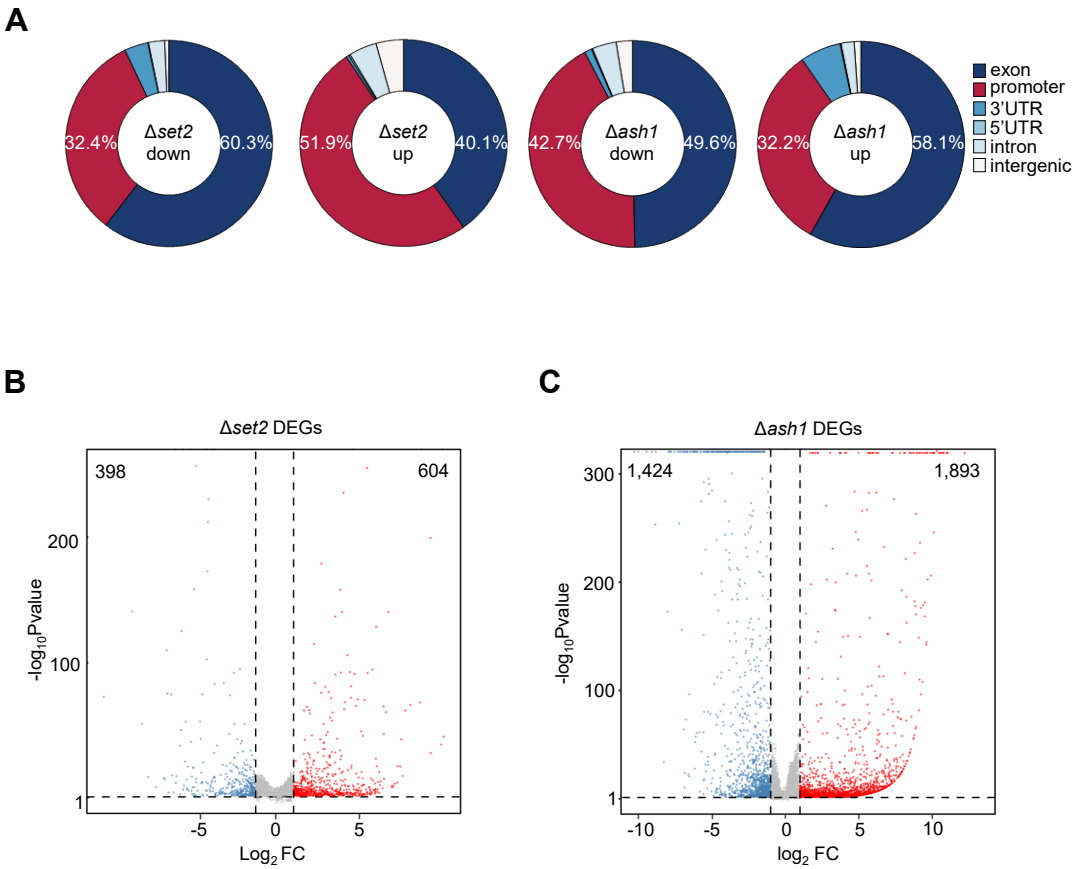

Supplemental Figure S5. H3K36me3 peak distribution and transcriptomic changes in Δ*set2* and Δ*ash1*. (A) Pie charts of increased/decreased H3K36me3 peaks across gene features in Δ*set2* and Δ*ash1*. (B, C) Volcano plots showing differentially expressed genes (DEGs) in Δ*set2* (B) and Δ*ash1* compared to PH-1.

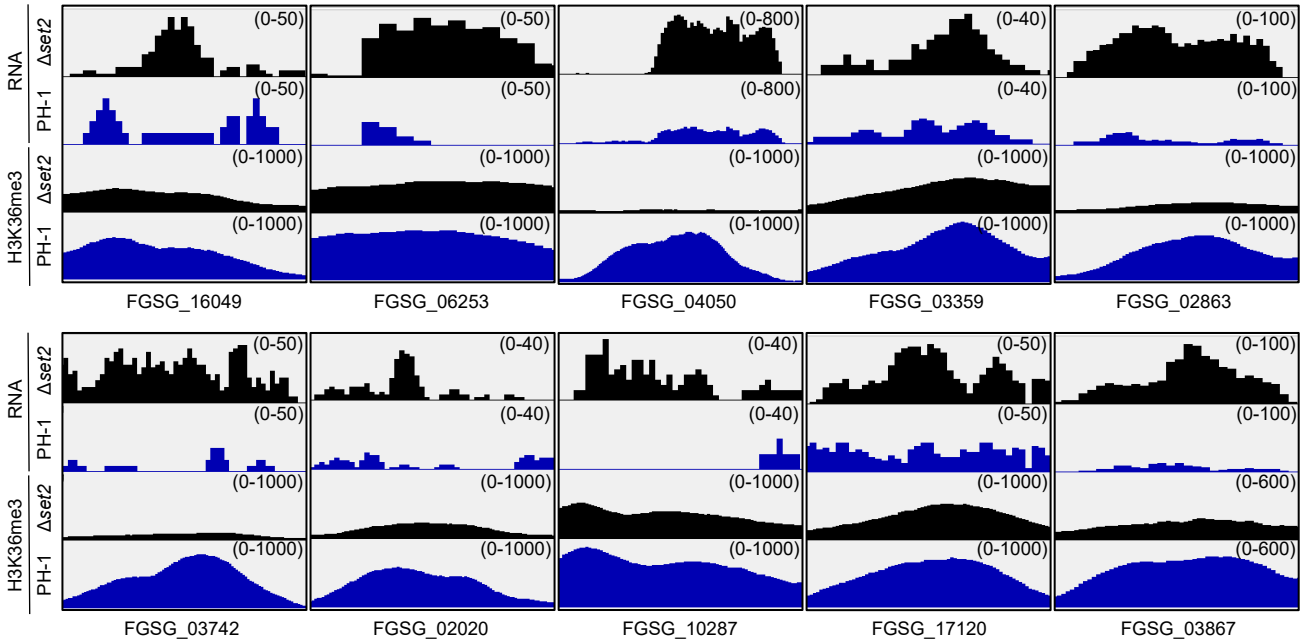

Supplemental Figure S6. IGV views of representative genes with cryptic transcription in Δ*set2*. IGV tracks of H3K36me3 and RNA-seq coverage for 10 representative genes with cryptic transcription in Δ*set2* compared to PH-1.

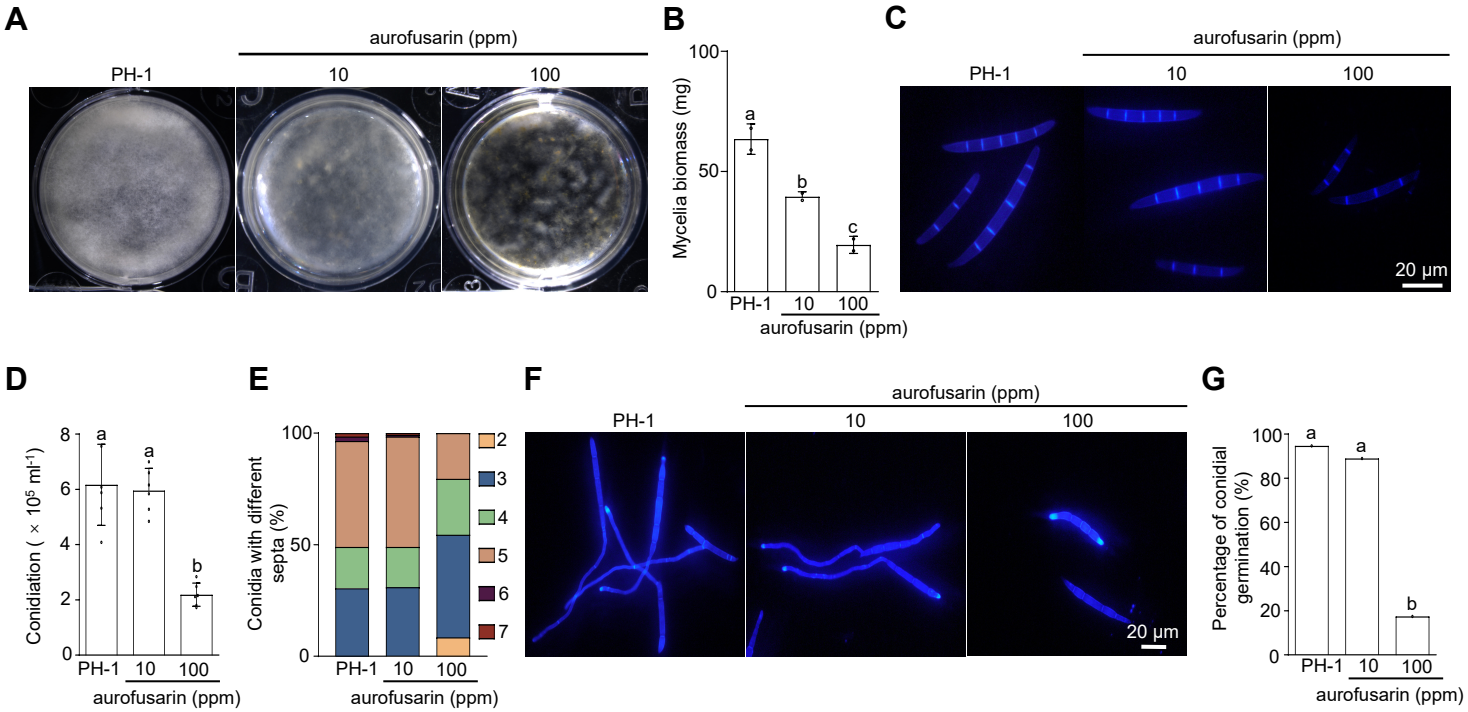

Supplemental Figure S7. Aurofusarin inhibits mycelia growth, conidiation, and germination in *F. graminearum*. (A) PH-1 conidia germinated in 2% sucrose for 5 h, then exposed to 10 or 100 ppm aurofusarin; cultures incubated at 25 °C in the dark for 48 h, and photographed. (B) Mycelial dry weight under different treatments in (A). Mycelia were harvested by filtration, dried, and weighed. Data are mean ± s.d (n = 2 biological replicates). (C) Conidial morphology after aurofusarin treatment. PH-1 was cultured in CMC liquid with 10 or 100 ppm aurofusarin at 25 °C ,180 rpm for 5 days. Conidia were stained with calcofluor white (CFW) and imaged by fluorescence microscopy. Scale bar, 20 μm. (D) Conidial production under each treatment. (E) Septa counts per conidium after treatment. (F) Morphology of germinated conidia exposed to aurofusarin. PH-1 conidia were incubated in 2% sucrose with 10 or 100 ppm aurofusarin for 5 h. Germinated conidia were stained with CFW and imaged. Scale bar, 20 μm. (G) Germination rates from ≥ 300 conidia per condition. Different letters indicate statistically significant differences (one-way ANOVA, Tukey's multiple comparisons test, $P < 0.05$).

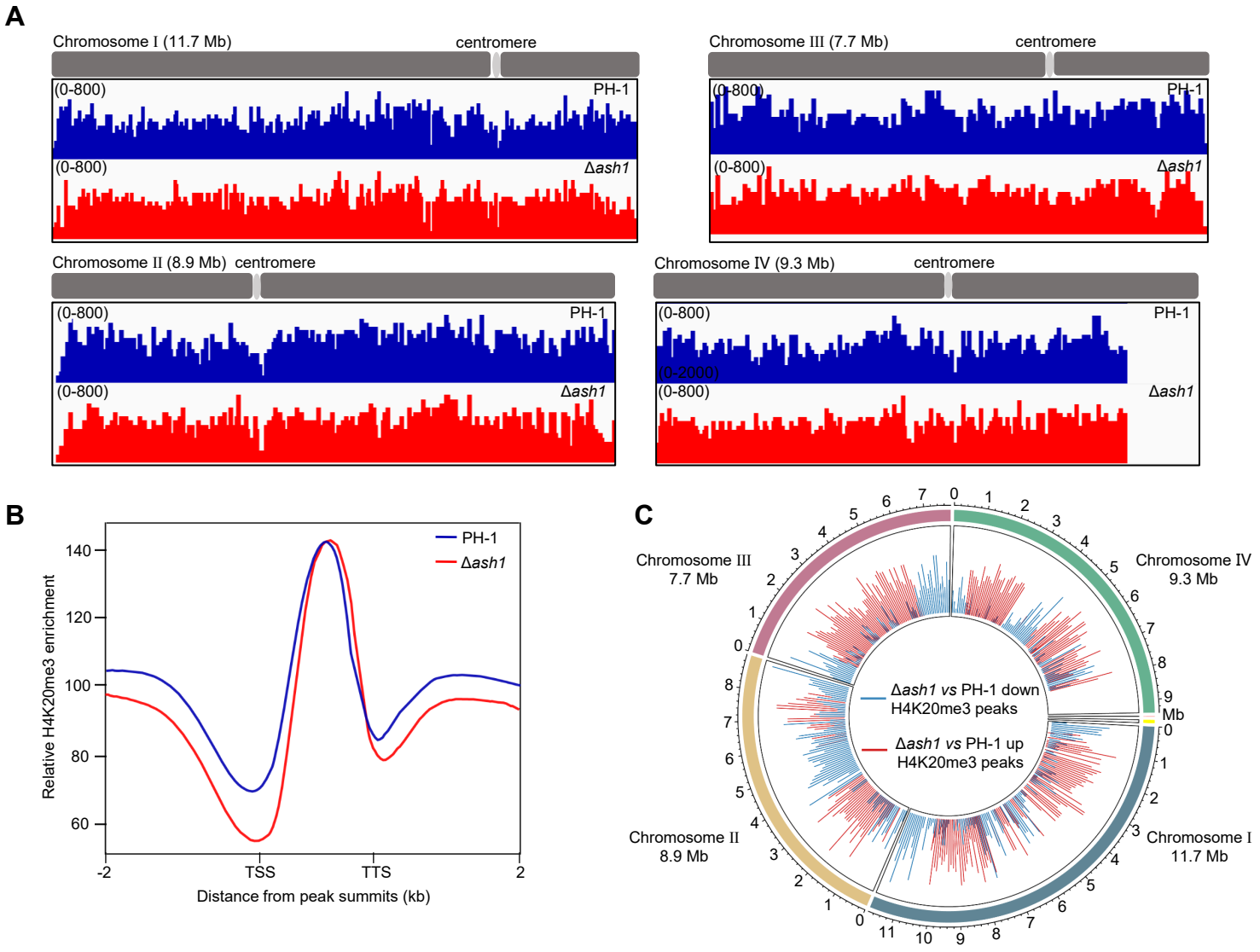

Supplemental Figure S8. Ash1 influences H4K20me3 deposition across distinct genomic regions in *F. graminearum*. (A) IGV tracks of H4K20me3 ChIP-seq across the four chromosomes in PH-1 and Δ*ash1*. Y-axis represents normalized read counts (reads per million, RPM). (B) Metagene plots of H4K20me3 over gene bodies and flanking intergenic regions in PH-1 and Δ*ash1*. TSS, transcription start site; TTS, transcription termination site. (C) Genome-wide H4K20me3 peaks with increased (red) or decreased (blue) enrichment in Δ*ash1 versus* PH-1.

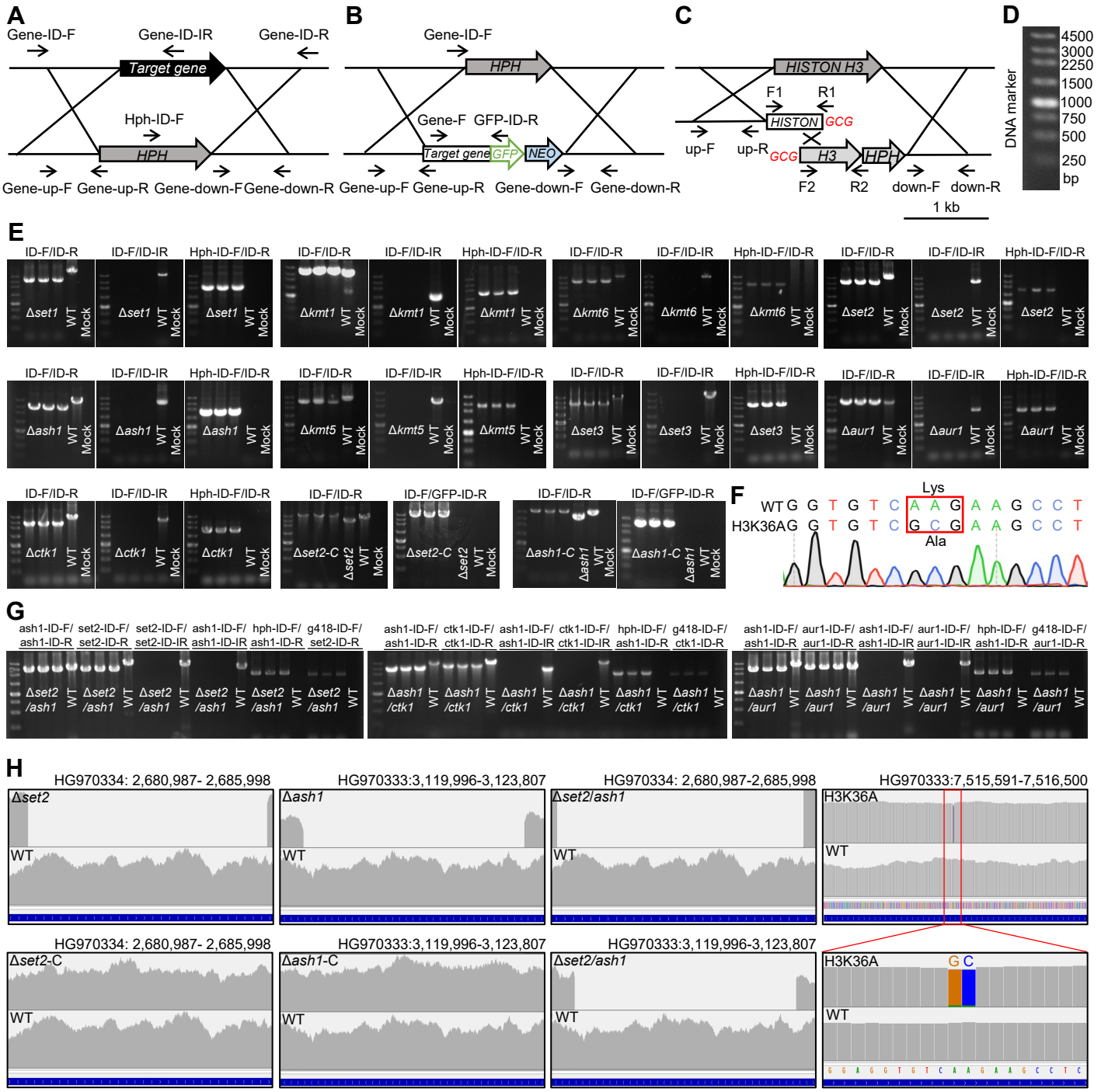

Supplemental Figure S9. Gene deletion, complementation, site-directed mutagenesis strategies, and mutant verification in *F. graminearum*. (A) Gene deletion strategy. The target gene was replaced by a hygromycin resistance cassette (*HPH*). PCR primers are indicated by arrows. (B) *In situ* complementation strategy. The construct contains the target gene, GFP, and a neomycin resistance gene (*NEO*). (C) Site-directed mutagenesis substituting histone H3K36 with alanine (H3K36A). (D) DNA ladder indicating fragment sizes for PCR verification. (E) PCR verification of deletion and complementation mutants. (F) Sanger sequencing confirmation of the H3K36A point mutation. (G) PCR verification of double-deletion mutants. (H) Whole-genome sequencing of Δ*set2*, Δ*ash1*, Δ*set2*/*ash1*, and H3K36A point mutants displayed as IGV tracks.